nature genetics

Recurrent somatic mutations of *PTPN1* in primary mediastinal B cell lymphoma and Hodgkin lymphoma

Jay Gunawardana[1,2], Fong Chun Chan[1,3], Adèle Telenius[1], Bruce Woolcock[1], Robert Kridel[1,2], King L Tan[1], Susana Ben-Neriah[1], Anja Mottok[1], Raymond S Lim[1], Merrill Boyle[1], Sanja Rogic[4], Lisa M Rimsza[5], Chrystelle Guiter[6], Karen Leroy[6–8], Philippe Gaulard[6–8], Corinne Haioun[7,8], Marco A Marra[9,10], Kerry J Savage[1], Joseph M Connors[1], Sohrab P Shah[2], Randy D Gascoyne[1,2] & Christian Steidl[1,2]

Classical Hodgkin lymphoma and primary mediastinal B cell lymphoma (PMBCL) are related lymphomas sharing pathological, molecular and clinical characteristics. Here we discovered by whole-genome and whole-transcriptome sequencing recurrent somatic coding-sequence mutations in the *PTPN1* gene. Mutations were found in 6 of 30 (20%) Hodgkin lymphoma cases, in 6 of 9 (67%) Hodgkin lymphoma–derived cell lines, in 17 of 77 (22%) PMBCL cases and in 1 of 3 (33%) PMBCL-derived cell lines, consisting of nonsense, missense and frameshift mutations. We demonstrate that *PTPN1* mutations lead to reduced phosphatase activity and increased phosphorylation of JAK-STAT pathway members. Moreover, silencing of *PTPN1* by RNA interference in Hodgkin lymphoma cell line KM-H2 resulted in hyperphosphorylation and overexpression of downstream oncogenic targets. Our data establish *PTPN1* mutations as new drivers in lymphomagenesis.

Hodgkin lymphoma accounts for 11% of all malignant lymphomas, with an annual worldwide incidence of 3 in 100,000 people. Despite advances in treatment and high curability, 20% of patients still succumb to their disease. Moreover, a similar proportion of patients are overtreated, leading to treatment-related consequences such as secondary malignancies and organ dysfunction[1]. PMBCL is a distinct subtype of aggressive B cell lymphoma that arises from thymic medullary B cells and characteristically presents as a mass in the anterior mediastinum. PMBCL affects predominantly young females[2] but can also occur in children and adolescents, displaying similar clinical and pathological characteristics as in adults[3]. With PMBCL recognized as a separate entity, its optimal treatment is currently the subject of debate, and variable treatment outcomes are reported. Because relapses after first-line therapies usually occur early and salvage therapies have been reported to have high failure rates, dose-intense chemotherapy regimens have been suggested. Moreover, combination therapies with rituximab immunotherapy and radiation therapy are currently being evaluated[4,5].

PMBCL and the nodular sclerosing subtype of Hodgkin lymphoma exhibit similar clinical, pathological and molecular features such as overlapping gene expression profiles as well as gains and losses of large chromosomal segments, specifically involving gains of 2p and 9p (refs. 6,7). Further, increased activation of Janus kinase–signal transducers and activators of transcription (JAK-STAT)[8–11] and nuclear factor (NF)-κB signaling has also been reported in both lymphoma subtypes[1,12]. However, the full spectrum of genetic changes underlying the malignant phenotypes of both diseases still remains to be uncovered.

Next-generation sequencing techniques have transformed the field of cancer genomics, allowing for rapid genome-wide characterization of single-nucleotide variants (SNVs), insertions-deletions (indels), structural genomic rearrangements and gene expression changes[13–16]. The study of cancer genomes at base-pair resolution in a variety of malignancies has yielded unprecedented insight into the complexity of primary and secondary alterations and has uncovered new and, in some cancer subtypes, highly recurrent driver alterations that produce cellular phenotypes that hold the promise of being targetable by new therapeutics[17,18].

To investigate somatic gene mutations in Hodgkin lymphoma and PMBCL, we used massively parallel next-generation sequencing to sequence the whole genomes and transcriptomes (RNA-seq) of two PMBCL index cases and analyzed eight additional cases by RNA-seq. We discovered new gene mutations in the *PTPN1* gene that were highly recurrent in our extension cohorts of Hodgkin lymphoma and PMBCL. *PTPN1* encodes PTP1B, a non-receptor-type member of the superfamily of protein tyrosine phosphatases, and, until now, recurrent somatic coding-sequence mutations of *PTPN1* had not been described in any

[1]Centre for Lymphoid Cancer, BC Cancer Agency, Vancouver, British Columbia, Canada. [2]Department of Pathology and Laboratory Medicine, University of British Columbia, Vancouver, British Columbia, Canada. [3]Bioinformatics Training Program, University of British Columbia, Vancouver, British Columbia, Canada. [4]Centre for High-Throughput Biology, University of British Columbia, Vancouver, British Columbia, Canada. [5]Department of Pathology, University of Arizona, Tucson, Arizona, USA. [6]INSERM U955, Créteil, France. [7]Université Paris Est, Créteil, France. [8]Département de Pathologie–Service d'Hématologie–Plateforme de Ressources Biologiques, Groupe Hospitalier Henri-MONDOR, Assistance Publique–Hôpitaux de Paris, Créteil, France. [9]Genome Sciences Centre, BC Cancer Agency, Vancouver, British Columbia, Canada. [10]Department of Medical Genetics, University of British Columbia, Vancouver, British Columbia, Canada. Correspondence should be addressed to C.S. (csteidl@bccancer.bc.ca).

Received 3 May 2013; accepted 24 January 2014; published online 16 February 2014; doi:10.1038/ng.2900

lymphoma. More broadly, strong genetic evidence for a role in human cancers is lacking, although both a tumor suppressor and oncogene function of *PTPN1* have been proposed[19,20]. Our data suggest that inactivating mutations contribute to the pathogenesis of PMBCL and Hodgkin lymphoma through activation of JAK-STAT signaling pathways.

RESULTS

Somatic mutations discovered by next-generation sequencing

To discover somatic mutations in PMBCL cancer genomes, we used whole-genome sequencing, comparing tumor genomes for two index cases to matched constitutional genomes. We generated 1,986,529,080 and 1,707,225,268 paired-end reads for subjects PM-2 and PM-7, respectively, of which 1,885,237,436 and 1,623,382,611 reads mapped to the reference human genome (94.9 and 95.1%; 188 and 162 Gb), resulting in average genomic coverage of 60 and 51.6×. The whole genomic landscapes for these index cases, consisting of copy number losses and gains and gene rearrangements, are shown in **Figure 1a**. Average intermutational distances were 317,246 and 280,509 bp for PM-2 and PM-7, respectively (**Fig. 1b**,**c**). We observed several genomic 'hotspot' regions with high mutation frequency in PM-7, including the *BCL6* oncogene[21,22] and the λ light-chain locus, known targets of somatic hypermutation. Somatic variant calling, including of SNVs and indels, identified 20,044 intronic (9,425 and 10,619), 32,565 intergenic (16,176 and 16,389), 22 5′ UTR (11 and 11), 81 3′ UTR (39 and 42) and 299 coding-region (148 and 151) mutations in the PM-2 and PM-7 genomes, respectively. Coding mutations and the distribution of nucleotide interchanges are shown in **Supplementary Tables 1–3** and **Figure 1d**,**e**, respectively. In both cases, we found mutations in two negative regulators of the JAK-STAT signaling pathway, *SOCS1* and *PTPN1*, and, because constitutive activation of JAK-STAT signaling has been reported as a hallmark feature of PMBCL, we focused on gene alteration in this pathway. Analysis of the transcriptome by RNA-seq of five additional cases and three PMBCL cell lines identified *PTPN1* mutations in two more cases (**Supplementary Tables 4–7**). The mutational patterns of gene alterations in the JAK-STAT signaling pathway are shown in **Figure 1f**, validating previously reported mutations of *SOCS1* and *STAT6* in PMBCL[23].

PTPN1 is mutated in PMBCL and Hodgkin lymphoma

As the mutation frequency of *PTPN1* in the discovery cohort was second only to that of mutations in *SOCS1*, a well-characterized tumor suppressor gene in PMBCL and Hodgkin lymphoma, we focused our study on *PTPN1* (refs. 24–27). We screened the complete coding sequence of *PTPN1*, comprising 10 exons, for genomic mutations in an additional 70 PMBCL samples by Sanger sequencing and deep amplicon sequencing. In total, after the exclusion of reported SNPs and silent mutations, we found 20 variants in our PMBCL cohort (18 mutations in 17 of 77 clinical samples and 2 mutations in 1 of 3 cell lines screened; **Supplementary Table 8a**), with some cases harboring multiple mutations. Because classical Hodgkin lymphoma is a closely related disease entity, we also screened 9 Hodgkin lymphoma–derived cell lines and 30 samples of Hodgkin Reed-Sternberg (HRS) cells, microdissected from classical Hodgkin lymphoma. A total of 12 mutations were discovered (6 in 30 microdissected HRS cells and 6 in 9 cell lines screened; **Supplementary Table 8b**). In summary, we found coding-sequence mutations in 30 of 119 (25%) clinical samples and cell lines of Hodgkin lymphoma and PMBCL. We observed 18 (60%) missense mutations, 4 (13.3%) frameshift mutations, 3 (10%)

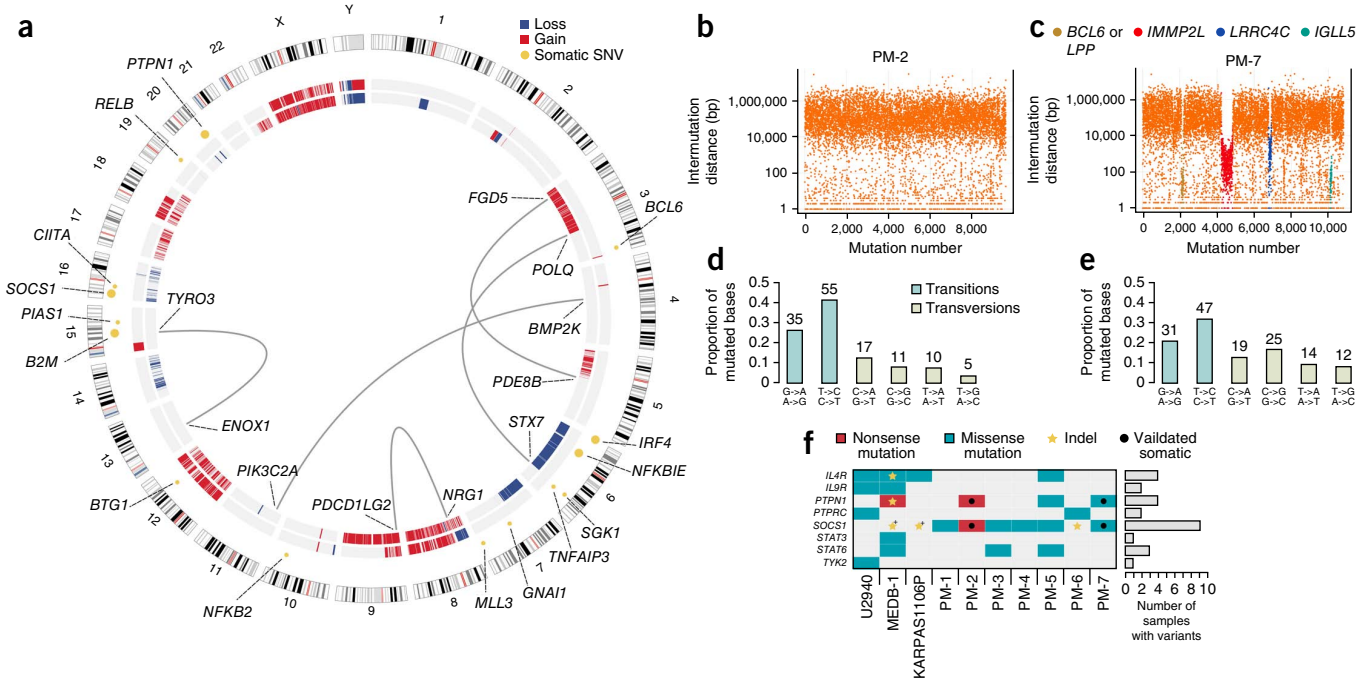

Figure 1 Results from whole-genome sequencing of two PMBCL tumors and germline DNA. (**a**) The outermost ring depicts the chromosome ideogram oriented clockwise, p terminus to q terminus. Centromeres are shown in red. The middle and innermost rings show copy number losses (blue) and gains (red) in PM-7 and PM-2, respectively. Genomic rearrangements are represented by arcs between chromosomes. Selected SNVs found in a single tumor library or in both libraries are annotated with smaller and larger circles, respectively. (**b**,**c**) Genome-wide intermutational distances in PM-2 (**b**) and PM-7 (**c**). (**d**,**e**) Distribution of somatic coding-sequence transition and transversion nucleotide interchanges in PM-2 (**d**) and PM-7 (**e**). The absolute number of nucleotide substitutions is shown above each bar. (**f**) Mutated genes in the JAK-STAT pathway discovered by whole-genome and whole-transcriptome sequencing (RNA-seq was performed on three PMBCL cell lines and seven tumor samples (PM-1–PM-7), and whole-genome sequencing was performed on PM-2 and PM-7 and on matched peripheral blood samples from the same individuals (+, previously reported[26]).

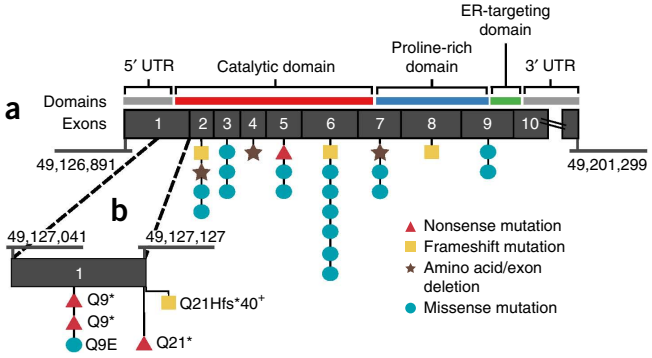

Figure 2 Locations of *PTPN1* mutations in Hodgkin lymphoma and PMBCL. (**a**) Distribution of *PTPN1* mutations in PMBCL cell lines ($n = 3$), PMBCL clinical samples ($n = 77$), Hodgkin lymphoma cell lines ($n = 9$) and Hodgkin lymphoma clinical samples ($n = 30$) identified by targeted Sanger sequencing. Variations in noncoding regions, reported SNPs and silent mutations are not shown. (**b**) Frequently mutated Gln9 and Gln21 residues encoded by exon 1. Gln21 is encoded by part of a splice donor site on this exon (+, putative translation).

single–amino acid deletions, 4 (13.3%) nonsense mutations and 1 (3.3%) promoter mutation. The distribution and frequency of mutations for each exon and the types of mutations observed are shown in **Figure 2a**. For all 6 Hodgkin lymphoma cases and 2 PMBCL cases with *PTPN1* mutations, we confirmed the identified mutations as somatic by sequencing constitutional DNA extracted from whole–lymph node tissue or peripheral blood. Mutation frequencies in PMBCL cell lines, PMBCL clinical cases, Hodgkin lymphoma cell lines and Hodgkin lymphoma clinical cases were 33%, 22%, 67% and 20%, respectively. Frequent mutations affecting Gln9 and Gln21 (NCBI reference sequence NP_002818.1) are suggestive of a potential mutational hotspot within the first exon (**Fig. 2b**) where aberrations might lead to premature inactivation of the protein, as was demonstrated by immunohistochemical staining in the PMBCL case PM-2 (**Fig. 3c**).

We next studied PTP1B protein expression by immunohistochemistry using formalin-fixed, paraffin-embedded and fresh-frozen tissues from Hodgkin lymphoma ($n = 215$) and PMBCL ($n = 143$) cases (**Supplementary Fig. 1**). Analysis of all available cases with known *PTPN1* mutation status identified a significant correlation between *PTPN1* mutations and decreased PTP1B protein expression. In PMBCL, the mean percentage of PTP1B-positive tumor cells in the group with wild-type *PTPN1* ($n = 33$) was 58.3% compared to 26.7% in the group with mutant *PTPN1* ($n = 9$; $P = 0.01$). In Hodgkin lymphoma, the mean percentage of PTP1B-positive tumor cells in the group with wild-type *PTPN1* ($n = 24$) was 63% compared to 35.8% in the group with mutant *PTPN1* ($n = 6$; $P = 0.04$) (**Supplementary Fig. 1a**,**b**). The distributions of PTP1B-positive tumor cells in PMBCL and Hodgkin lymphoma tissue samples are shown in **Supplementary Figure 1c**,**d**, and representative immunohistochemistry images of PMBCL and Hodgkin lymphoma tissue sections exhibiting variable PTP1B staining are shown in **Figure 3**. We also sought to determine whether *PTPN1* mutations were associated with patient survival. Kaplan-Meier survival analysis of individuals with PMBCL and Hodgkin lymphoma showed no significant differences in clinical outcome between groups with wild-type and mutated *PTPN1* ($P > 0.05$; **Supplementary Figs. 2** and **3**).

In addition to inactivating mutations that were correlated to loss of expression by immunohistochemistry (**Fig. 3c**) in clinical samples, we also found copy number losses in cell lines Karpas-1106P and U-H01 by FISH (**Supplementary Fig. 4**). However, focal *PTPN1* copy number changes were not found in any clinical samples studied by FISH (9 Hodgkin lymphoma and 13 PMBCL cases). Of interest, in U-H01, the remaining *PTPN1* allele contained a deletion of exons 2–8 (chr. 20: 49,153,833–49,197,665), leading to complete loss of PTP1B protein expression and transcript levels (**Supplementary Fig. 5a**,**b**). Moreover, the described nonsense and frameshift mutations of *PTPN1* in cell lines MedB-1 (in *trans*-allelic configuration; **Supplementary Fig. 6**) and L-1236, as well as the multiple-exon deletion in SUP-HD1, are consistent with complete loss or reduced expression of C-terminal PTP1B by protein blotting compared to a lymphoblastoid positive control cell line (LCL) (**Supplementary Fig. 5a**). However, absolute *PTPN1* transcript and PTP1B protein levels varied among cell lines and did not consistently correlate with protein expression, possibly owing to post-transcriptional and post-translational regulatory mechanisms.

PTPN1 mutations decrease phosphatase activity

To evaluate how phosphatase activity was affected by the observed nonsense and missense mutations, we expressed wild-type PTP1B or mutant PTP1B with p.Gln9*, p.Arg156*, p.Ala69Val, p.Met74Leu, p.Val184Asp and p.Met282Leu alterations in engineered human embryonic kidney 293 cells expressing STAT6 (HEK 293–STAT6) and a STAT6-inducible reporter gene (secreted embryonic alkaline phosphatase, *SEAP*). When cells were stimulated with human interleukin-4 (IL-4), expression of wild-type PTP1B resulted in

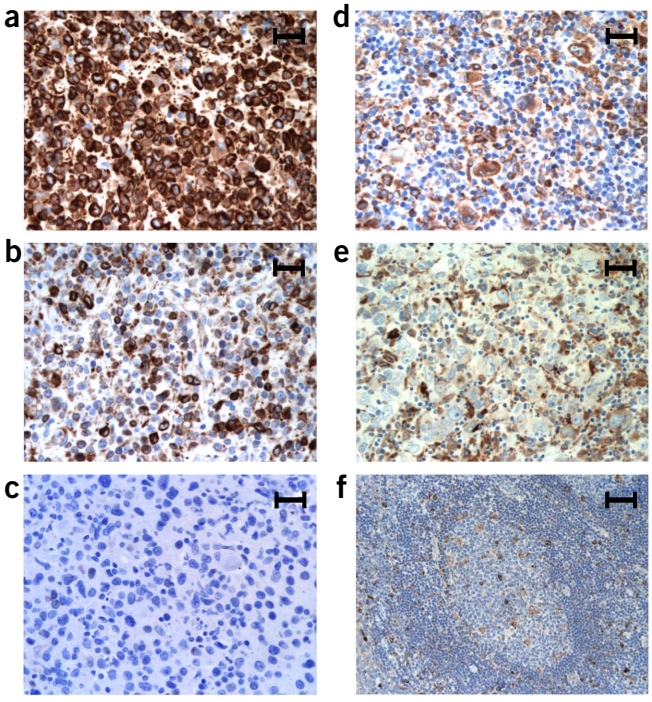

Figure 3 Immunohistochemical analysis of PTP1B expression in lymph node biopsy samples from Hodgkin lymphoma ($n = 215$) and PMBCL ($n = 143$). Representative images of sections stained with a monoclonal antibody against PTP1B are shown (original magnification of 400× (scale bars, 25 µm; **a**–**e**) and 200× (scale bar, 50 µm; **f**)). (**a**–**c**) PMBCL samples expressing wild-type PTP1B (PM-15) (**a**), Gly381Ser PTP1B (PM-9) (**b**) and Gln21* PTP1B (PM-2) (**c**). (**d**,**e**) Hodgkin lymphoma samples expressing wild-type PTP1B (HD-99) (**d**) and Met109del PTP1B (HD-42) (**e**). (**f**) Normal tonsil tissue with a germinal center shown for comparison.

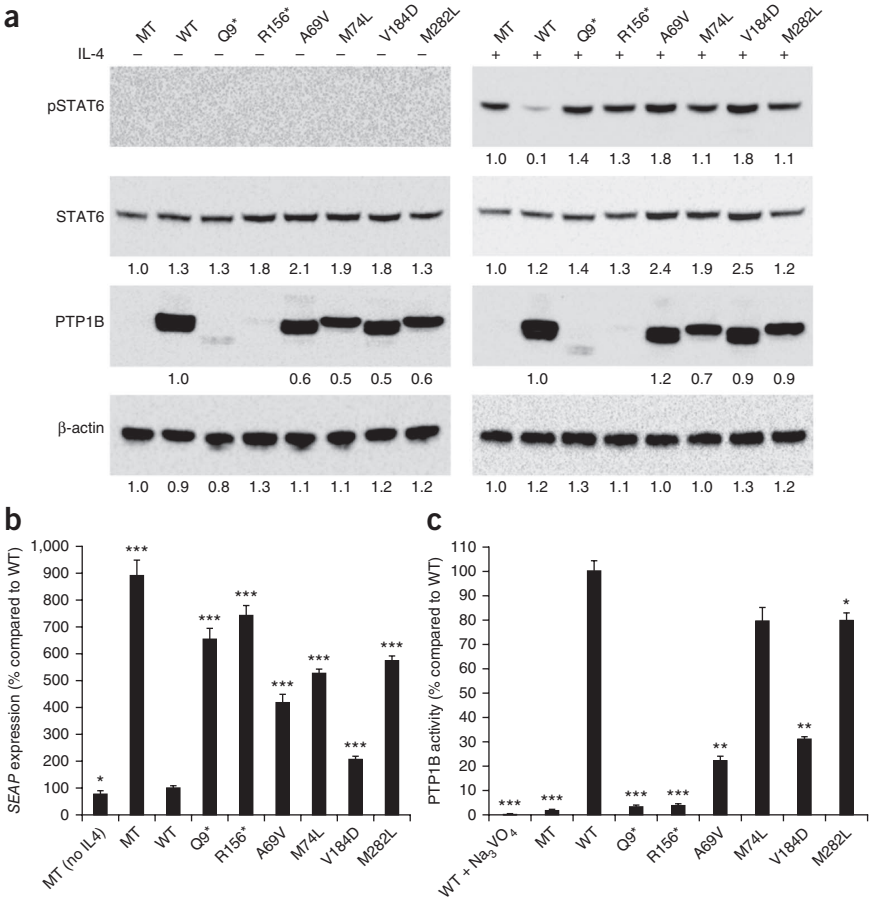

Figure 4 Expression of PTP1B mutants in HEK 293–STAT6 cells. (**a**) Levels of phosphorylated STAT6 (pSTAT6) in HEK 293–STAT6 cells transfected with constructs expressing wild-type or mutant PTP1B determined by protein blotting. Protein lysates were prepared from cell cultures treated with or without 20 ng/ml IL-4. Relative densitometric values (shown for each band) were normalized against the levels of the internal control β-actin. (**b**) Activated STAT6-dependent *SEAP* reporter gene expression in transfected cells. Each sample was run in triplicate. Each value represents the average of two independent experiments. Error bars, s.d. (**c**) PTP1B activity levels in lysates from transfected cells without IL-4 as determined by catalysis of the tyrosine phosphatase substrate DADEY(PO_3)LIPQQG. Each sample was run in triplicate. Each value represents the average of two independent experiments. Error bars, s.d. (MT, mock expression vector only; WT, wild type; $^{***}P < 0.001$, $^{**}P < 0.01$ and $^{*}P < 0.05$ compared to wild type.)

marked dephosphorylation of STAT6 compared to the empty vector control (relative densitometric value of 0.1). In contrast, we observed sustained phosphorylation of STAT6 with the expression of all mutants in comparison to the empty vector control (relative densitometric values: p.Gln9*, 1.4; p.Arg156*, 1.3; p.Ala69Val, 1.8; p.Met74Leu, 1.1; p.Val184Asp, 1.8; p.Met282Leu, 1.1; **Fig. 4a**), confirming these alterations as deleterious. Similarly, analysis of activated STAT6-dependent *SEAP* reporter gene expression in these mutant cells showed JAK-STAT pathway activation under IL-4 stimulation (percentage of *SEAP* expression compared to wild type: empty vector, 891%; p.Gln9*, 656%; p.Arg156*, 742%; p.Ala69Val, 417%; p.Met74Leu, 527%; p.Val184Asp, 208%; p.Met282Leu, 575%; **Fig. 4b**). Furthermore, we observed no phosphatase activity for the nonsense mutants and a moderate but significant reduction in phosphatase activity for the missense mutants using a tyrosine phosphatase–specific substrate (percentage of phosphatase activity compared to wild type: p.Gln9* 3.3%; p.Arg156*, 3.7%; p.Ala69Val, 22.1%; p.Met74Leu, 79.7%; p.Val184Asp, 31.3%; p.Met282Leu, 79.6%; **Fig. 4c**).

PTPN1 knockdown hyperphosphorylates JAK-STAT proteins

To study the functional relevance of the predicted inactivating *PTPN1* mutations, we generated a knockdown Hodgkin lymphoma cell line (KMH2-PTPN1-KD) in which *PTPN1* mRNA expression was silenced by lentiviral transduction of a short hairpin RNA (shRNA) construct targeting *PTPN1*. Knockdown efficiency was determined by quantitative RT-PCR (qRT-PCR) (34% residual mRNA; **Fig. 5a**) and by protein blotting, which showed minimal PTP1B protein expression compared to cells transduced with a non-silencing construct (KMH2-NS) (**Fig. 5b**). To determine whether silencing of *PTPN1* affected JAK-STAT signaling, we analyzed cell lysates by protein blotting for hyperphosphorylation of members of the JAK-STAT pathway. We also treated cells with recombinant IL-4 in order to stimulate the pathway to enhance detectable changes in phosphorylation. In KMH2-PTPN1-KD cells treated with IL-4 compared to negative-control cells treated with IL-4, we observed increased phosphorylation of STAT3, STAT5, STAT6, JAK1 and JAK2 (densitometric values of 12.6 versus 1.5, 2.8 versus 1.0, 1.5 versus 0.7, 7.0 versus 1.0, and 3.8 versus 1.7, respectively). In addition, we detected increased levels of JAK1 (2.9 versus 1.4). We also observed increased phosphorylation of the prosurvival protein AKT (5.1 versus 2.0), consistent with similar findings in mouse fibroblasts[28].

To investigate genome-wide gene expression changes in KMH2-PTPN1-KD versus KMH2-NS cells, we performed gene expression profiling using human genome U133 plus 2.0 arrays. We found 2,463 differentially expressed probe sets, of which 1,807 were found to be upregulated (fold change > 1.25 compared to KMH2-NS cells) and 656 were found to be downregulated (fold change < 0.8 compared to KMH2-NS cells; **Supplementary Table 9**). Because STAT3 showed the most pronounced changes in phosphorylation in our silenced cells and because of its reported effects on cell proliferation and survival[29], we looked for STAT3 downstream targets in our differentially expressed genes. Thirty-eight of 50 (76%; sign-test $P = 0.0003$) known STAT3-responsive genes were upregulated in *PTPN1* knockdown cells (**Fig. 5c**)[30]. Of note, two members of the gene family of ATP-binding cassette (ABC) transmembrane transporters were overexpressed in KMH2-PTPN1-KD cells—*ABCA8* (fold change = 5.2) and *ABCB1* (fold change = 1.5)—compared to KMH2-NS cells (**Supplementary Table 9**), with the latter being implicated in drug resistance in a number of malignancies[31]. Molecular pathway analysis of over- and underexpressed genes using Ingenuity Pathway Analysis (Ingenuity Systems) confirmed alterations in JAK-STAT–mediated cytokine signaling (false discovery rate (FDR)-adjusted $P = 0.004$) and showed defects in B cell development (FDR-adjusted $P = 0.004$), respectively (**Supplementary Table 10a–d**). Gene set enrichment analysis of differentially expressed genes showed enrichment of genes involved

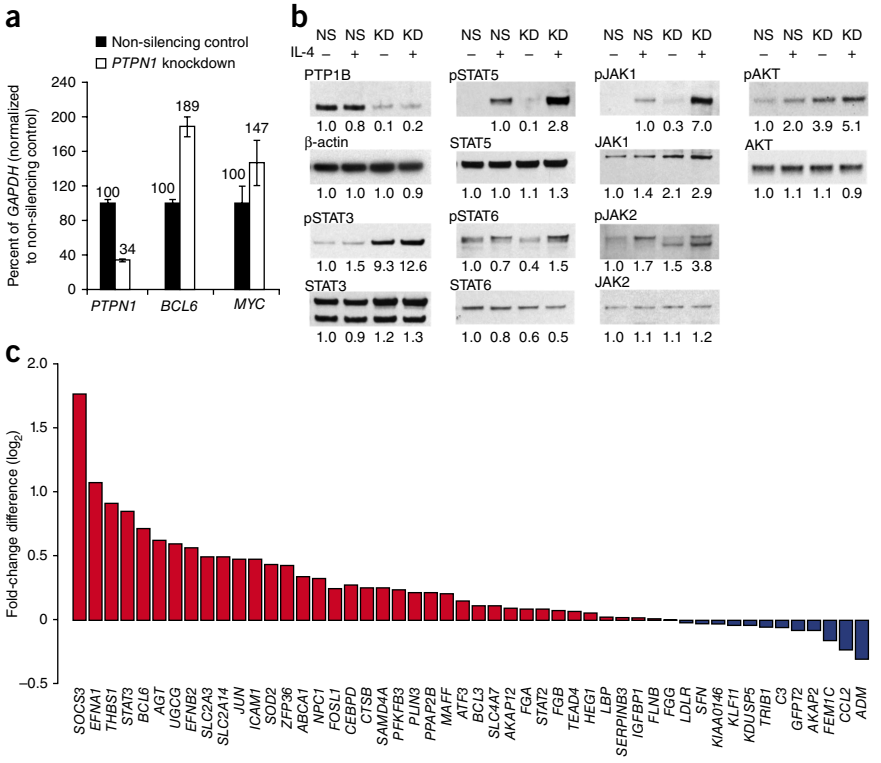

Figure 5 Activation of JAK-STAT in a *PTPN1*-silenced Hodgkin lymphoma cell line (KM-H2). (**a**) Quantitative PCR performed on RNA isolated from *PTPN1* knockdown and non-silencing cells using TaqMan assay probes. Each sample was run in triplicate. Each value represents the average of three independent experiments. Error bars, s.d. (**b**) Hyperphosphorylation of JAK (pJAK1, pJAK2) and STAT (pSTAT3, pSTAT5, pSTAT6) proteins determined by protein blotting in the KM-H2 cell line with shRNA-mediated knockdown of *PTPN1*. Protein lysates from non-silencing (NS) and knockdown (KD) cells were prepared from cell cultures treated with or without 10 ng/ml IL-4. Relative densitometric values (shown for each band) were normalized against levels of the internal control β-actin. (**c**) Gene expression profiling of RNA isolated from *PTPN1* knockdown and non-silencing cells on an HG U133 Plus 2.0 array. Differentially expressed genes were compared against 50 known STAT3-responsive genes. Thirty-eight genes overlapped with our gene cohort ($P = 0.0003$). Only 2 of 10,000 random permutations had a value of ≥38 ($P = 0.0002$). Fold-change differences were compared against the non-silencing control.

in tumorigenesis and cytokine, growth receptor and JAK-STAT signaling (**Supplementary Fig. 7**). Moreover, the upregulated oncogenes *BCL6* and *MYC* in silenced cells were validated by qRT-PCR (189% and 147% of the levels in KMH2-NS cells, respectively; **Fig. 5a**).

DISCUSSION

Using whole-genome and whole-transcriptome sequencing approaches, we identified somatic coding-sequence mutations in the non-receptor-type tyrosine phosphatase gene *PTPN1*, a gene that has not previously been described as being recurrently mutated in lymphoid cancers. By targeted Sanger sequencing, we found that *PTPN1* mutations were highly recurrent in the molecularly related B cell lymphoma entities PMBCL and Hodgkin lymphoma. The pattern of identified mutations consisting of nonsense, missense and frameshift changes and single–amino acid deletions with a hotspot region in the first exon is indicative of loss of function of a negative regulator of oncogenic JAK-STAT activation. As demonstrated, mutated *PTPN1* yields functionally deleterious or hypomorphic phosphatases that result in deregulated STAT phosphorylation. Moreover, heterozygous and homozygous deletions in some cell lines, as well as loss of protein detectable by immunohistochemistry and protein blotting in samples harboring *PTPN1* coding-sequence mutations, are consistent with classical mechanisms of inactivation of a tumor suppressor gene in the context of these B cell lymphomas.

The role of *PTPN1* expression in human cancer is controversial. Although recurrent coding-sequence mutations have not previously been described, both up- and downregulation of *PTPN1* gene expression have been linked to carcinogenesis, suggesting both tumor suppressor gene and oncogene functions depending on the cellular context[32–37]. Protein tyrosine phosphatases act as a molecular 'switch' to maintain the homeostatic balance of receptor tyrosine kinase signaling by removing phosphate moieties from phosphorylated proteins. This critical regulation mediates diverse cellular processes such as cell proliferation, adhesion, migration and immune and hormonal responses[38,39]. Alterations in *PTPN2* (encoding TC-PTP) were identified in T cell acute lymphoblastic leukemia (T-ALL), where mutations and focal deletions led to hyperphosphorylation of JAK-STAT signaling molecules; however, recurrent coding-sequence mutations could not be established in B cell lymphoma[40,41]. More recently, an elegant study of triple-negative breast cancer demonstrated the suppressive role of *PTPN12* in inhibiting the HER2 and EGFR oncogenic kinases in order to restrain mammary epithelial cell proliferation and transformation[42]. However, not all members of the PTP family exhibit tumor-suppressive properties. Gain-of-function mutations in the proto-oncogene *PTPN11* can aberrantly activate the RAS-MAPK cascade in myeloid leukemias[43].

Our report of *PTPN1* coding-sequence mutations in B cell lymphomas describes another PTP family member as being critically involved in oncogenesis. PTP1B is ubiquitously expressed in human tissues and is found in the cytoplasm, localized within the endoplasmic reticulum. It dephosphorylates tyrosine residues on many growth factor receptors (for example, EGFR, PDGFR and HGFR), activated kinases (for example, SRC, p210BCR-ABL, TYK2 and JAK2) and transcription factors (for example, STAT5) to maintain cellular homeostasis[19,44]. So far, the functional role of PTP1B expression in lymphomagenesis has only been studied in a *Tp53* and *Ptpn1* double-null mouse model where increased accumulation of B cells in the bone marrow and lymph nodes and decreased survival rates were observed[45]. This lymphoma-like phenotype, together with our observation of increased phosphorylation of AKT and JAK-STAT pathway members as well as abrogated or diminished phosphatase activity resulting in sustained STAT6 activation, is highly indicative of a tumor-promoting phenotype in the absence of functional PTP1B. Moreover, upregulation of the classical lymphoma oncogenes *BCL6* and *MYC* in KM-H2 cells with *PTPN1* knockdown might in part explain the tissue specificity of B cell lymphoma. However, the absence of *PTPN1* mutations in other lymphoma subtypes that were previously studied by next-generation sequencing[46] suggests a synergy of *PTPN1* mutations with other somatic changes or specific cell of origin–related expression programs. In particular, it is likely that the mutations in *PTPN1*

synergize with other driver mutations known to be involved in the pathogenesis of Hodgkin lymphoma and PMBCL (mutations in *SOCS1* and *STAT6*) that contribute to aberrant JAK-STAT signaling. Our results demonstrate a significant correlation of *PTPN1* mutations with diminished PTP1B expression in clinical samples and active JAK-STAT signaling *in vitro*. However, additional studies in a larger cohort are needed to investigate the mutational patterns of JAK-STAT signaling genes, including *PTPN1* mutations, and to correlate these patterns with gene expression phenotypes. These studies will also clarify whether PTP1B immunohistochemistry can be used as a reasonable surrogate for *PTPN1* mutations in clinical samples.

Interestingly, we identified the multidrug resistance gene *ABCB1* as being upregulated in KM-H2 *PTPN1* knockdown cells. ABCB1 is a prominent family member of the ABC-containing transmembrane transporters that confer drug resistance in multiple cancers[47,48]. Of note, lack of *PTPN1* has been implicated in the treatment resistance of chronic myeloid leukemia[32]. Although only a trend toward inferior progression-free survival was observed in our PMBCL cases with *PTPN1* mutations, further validation studies in larger homogeneously treated Hodgkin lymphoma and PMBCL cohorts are needed to evaluate the prognostic value of *PTPN1* mutations in these diseases. Lastly, the identification of a specific lymphoma phenotype, including drug resistance, linked to these mutations harbors potential for the development of targeted treatment approaches in this molecularly characterized subgroup of B cell lymphomas.

In summary, we have discovered recurrent somatic mutations in *PTPN1*, a phosphatase that negatively regulates kinase activity in Hodgkin lymphoma and PMBCL. Our data suggest *PTPN1* mutations as new oncogenic drivers in these lymphomas, with implications for future treatment strategies.

URLs. Ingenuity, http://www.ingenuity.com/; R Project, http://www.R-project.org/; Deutsche Sammlung von Mikroorganismen und Zellkulturen (DSMZ), http://www.dsmz.de/; deStruct, https://code.google.com/p/destruct.

METHODS

Methods and any associated references are available in the online version of the paper.

Accession codes. Sequencing data have been deposited in the European Genome-phenome Archive (EGA) under accession EGAS00001000554, and gene expression data have been deposited in the Gene Expression Omnibus (GEO) under accession GSE54157.

Note: Any Supplementary Information and Source Data files are available in the online version of the paper.

ACKNOWLEDGMENTS

We thank the BC Cancer Foundation and the Canada Foundation for Innovation for their support. We also thank T. Van Tol, M. Drake, R. Tong, the Genome Sciences Centre (GSC) production group and the Center for Translational and Applied Genomics (CTAG) for excellent technical support. This work is supported by a research grant from the Leukemia & Lymphoma Society of Canada (LLSC) and by a Terry Fox Research Institute team grant (1023) to C.S. and a Scholarship award from the Michael Smith Foundation for Health Research (MSFHR) to C.S. R.D.G. is supported by a Canadian Institutes of Health Research (CIHR) grant (178536) and a Terry Fox Foundation program project grant (019001). A.M. is supported by a fellowship award from the Mildred Scheel Cancer Foundation. R.K. is supported by fellowship awards from CIHR, MSFHR and the University of British Columbia.

AUTHOR CONTRIBUTIONS

J.G. designed and performed the research, analyzed and interpreted data and wrote the manuscript. A.T., B.W., K.L.T., S.B.-N., A.M., M.B., R.K. and C.G. performed experiments and interpreted data. F.C.C., R.S.L. and S.R. analyzed data from whole-genome sequencing, RNA-seq and amplicon sequencing. C.H., K.L., L.M.R. and P.G. provided study material and interpreted results. K.J.S., M.A.M. and S.P.S. interpreted data. J.M.C. and R.D.G. curated the lymphoma database, interpreted data and reviewed the manuscript. C.S. designed the research, analyzed and interpreted data and wrote the manuscript.

COMPETING FINANCIAL INTERESTS

The authors declare no competing financial interests.

1. Steidl, C., Connors, J.M. & Gascoyne, R.D. Molecular pathogenesis of Hodgkin's lymphoma: increasing evidence of the importance of the microenvironment. *J. Clin. Oncol.* **29**, 1812–1826 (2011).
2. Johnson, P.W. & Davies, A.J. Primary mediastinal B-cell lymphoma. *Hematology (Am Soc Hematol Educ Program)* **2008**, 349–358 (2008).
3. Oschlies, I. *et al.* Clinical, pathological and genetic features of primary mediastinal large B-cell lymphomas and mediastinal gray zone lymphomas in children. *Haematologica* **96**, 262–268 (2011).
4. Rieger, M. *et al.* Primary mediastinal B-cell lymphoma treated with CHOP-like chemotherapy with or without rituximab: results of the Mabthera International Trial Group study. *Ann. Oncol.* **22**, 664–670 (2011).
5. Dunleavy, K. *et al.* Dose-adjusted EPOCH-rituximab therapy in primary mediastinal B-cell lymphoma. *N. Engl. J. Med.* **368**, 1408–1416 (2013).
6. Kimm, L.R. *et al.* Frequent occurrence of deletions in primary mediastinal B-cell lymphoma. *Genes Chromosom. Cancer* **46**, 1090–1097 (2007).
7. Savage, K.J. Primary mediastinal large B-cell lymphoma. *Oncologist* **11**, 488–495 (2006).
8. Skinnider, B.F. *et al.* Signal transducer and activator of transcription 6 is frequently activated in Hodgkin and Reed-Sternberg cells of Hodgkin lymphoma. *Blood* **99**, 618–626 (2002).
9. Guiter, C. *et al.* Constitutive STAT6 activation in primary mediastinal large B-cell lymphoma. *Blood* **104**, 543–549 (2004).
10. Kube, D. *et al.* STAT3 is constitutively activated in Hodgkin cell lines. *Blood* **98**, 762–770 (2001).
11. Scheeren, F.A. *et al.* IL-21 is expressed in Hodgkin lymphoma and activates STAT5: evidence that activated STAT5 is required for Hodgkin lymphomagenesis. *Blood* **111**, 4706–4715 (2008).
12. Steidl, C. & Gascoyne, R.D. The molecular pathogenesis of primary mediastinal large B-cell lymphoma. *Blood* **118**, 2659–2669 (2011).
13. Ding, L. *et al.* Clonal evolution in relapsed acute myeloid leukaemia revealed by whole-genome sequencing. *Nature* **481**, 506–510 (2012).
14. Morin, R.D. *et al.* Frequent mutation of histone-modifying genes in non-Hodgkin lymphoma. *Nature* **476**, 298–303 (2011).
15. Shah, S.P. *et al.* The clonal and mutational evolution spectrum of primary triple-negative breast cancers. *Nature* **486**, 395–399 (2012).
16. Steidl, C. *et al.* MHC class II transactivator *CIITA* is a recurrent gene fusion partner in lymphoid cancers. *Nature* **471**, 377–381 (2011).
17. Shah, S.P. *et al.* Mutation of *FOXL2* in granulosa-cell tumors of the ovary. *N. Engl. J. Med.* **360**, 2719–2729 (2009).
18. Tiacci, E. *et al.* *BRAF* mutations in hairy-cell leukemia. *N. Engl. J. Med.* **364**, 2305–2315 (2011).
19. Dubé, N. & Tremblay, M.L. Beyond the metabolic function of PTP1B. *Cell Cycle* **3**, 550–553 (2004).
20. Yip, S.C., Saha, S. & Chernoff, J. PTP1B: a double agent in metabolism and oncogenesis. *Trends Biochem. Sci.* **35**, 442–449 (2010).
21. Pasqualucci, L. *et al.* BCL-6 mutations in normal germinal center B cells: evidence of somatic hypermutation acting outside Ig loci. *Proc. Natl. Acad. Sci. USA* **95**, 11816–11821 (1998).
22. Popov, S.W. *et al.* Target sequence accessibility limits activation-induced cytidine deaminase activity in primary mediastinal B-cell lymphoma. *Cancer Res.* **67**, 6555–6564 (2007).
23. Ritz, O. *et al.* Recurrent mutations of the STAT6 DNA binding domain in primary mediastinal B-cell lymphoma. *Blood* **114**, 1236–1242 (2009).
24. Melzner, I. *et al.* Biallelic mutation of *SOCS-1* impairs JAK2 degradation and sustains phospho-JAK2 action in the MedB-1 mediastinal lymphoma line. *Blood* **105**, 2535–2542 (2005).
25. Mottok, A. *et al.* Inactivating *SOCS1* mutations are caused by aberrant somatic hypermutation and restricted to a subset of B-cell lymphoma entities. *Blood* **114**, 4503–4506 (2009).
26. Ritz, O. *et al.* STAT6 activity is regulated by SOCS-1 and modulates BCL-XL expression in primary mediastinal B-cell lymphoma. *Leukemia* **22**, 2106–2110 (2008).
27. Weniger, M.A. *et al.* Mutations of the tumor suppressor gene *SOCS-1* in classical Hodgkin lymphoma are frequent and associated with nuclear phospho-STAT5 accumulation. *Oncogene* **25**, 2679–2684 (2006).
28. Lu, X. *et al.* PTP1B is a negative regulator of interleukin 4–induced STAT6 signaling. *Blood* **112**, 4098–4108 (2008).

29. Ding, B.B. *et al.* Constitutively activated STAT3 promotes cell proliferation and survival in the activated B-cell subtype of diffuse large B-cell lymphomas. *Blood* **111**, 1515–1523 (2008).
30. Dauer, D.J. *et al.* Stat3 regulates genes common to both wound healing and cancer. *Oncogene* **24**, 3397–3408 (2005).
31. Gottesman, M.M., Fojo, T. & Bates, S.E. Multidrug resistance in cancer: role of ATP-dependent transporters. *Nat. Rev. Cancer* **2**, 48–58 (2002).
32. Koyama, N. *et al.* Inhibition of phosphotyrosine phosphatase 1B causes resistance in BCR-ABL–positive leukemia cells to the ABL kinase inhibitor STI571. *Clin. Cancer Res.* **12**, 2025–2031 (2006).
33. Nanney, L.B., Davidson, M.K., Gates, R.E., Kano, M. & King, L.E. Jr. Altered distribution and expression of protein tyrosine phosphatases in normal human skin as compared to squamous cell carcinomas. *J. Cutan. Pathol.* **24**, 521–532 (1997).
34. Warabi, M., Nemoto, T., Ohashi, K., Kitagawa, M. & Hirokawa, K. Expression of protein tyrosine phosphatases and its significance in esophageal cancer. *Exp. Mol. Pathol.* **68**, 187–195 (2000).
35. Wiener, J.R. *et al.* Overexpression of the tyrosine phosphatase PTP1B is associated with human ovarian carcinomas. *Am. J. Obstet. Gynecol.* **170**, 1177–1183 (1994).
36. Zhai, Y.F. *et al.* Increased expression of specific protein tyrosine phosphatases in human breast epithelial cells neoplastically transformed by the *neu* oncogene. *Cancer Res.* **53**, 2272–2278 (1993).
37. Wiener, J.R. *et al.* Overexpression of the protein tyrosine phosphatase PTP1B in human breast cancer: association with $p185^{c\text{-}erbB\text{-}2}$ protein expression. *J. Natl. Cancer Inst.* **86**, 372–378 (1994).
38. Blume-Jensen, P. & Hunter, T. Oncogenic kinase signalling. *Nature* **411**, 355–365 (2001).
39. Lim, W.A. & Pawson, T. Phosphotyrosine signaling: evolving a new cellular communication system. *Cell* **142**, 661–667 (2010).
40. Kleppe, M. *et al.* Deletion of the protein tyrosine phosphatase gene *PTPN2* in T-cell acute lymphoblastic leukemia. *Nat. Genet.* **42**, 530–535 (2010).
41. Kleppe, M. *et al.* Mutation analysis of the tyrosine phosphatase *PTPN2* in Hodgkin's lymphoma and T-cell non-Hodgkin's lymphoma. *Haematologica* **96**, 1723–1727 (2011).
42. Sun, T. *et al.* Activation of multiple proto-oncogenic tyrosine kinases in breast cancer via loss of the *PTPN12* phosphatase. *Cell* **144**, 703–718 (2011).
43. Tartaglia, M. *et al.* Somatic mutations in *PTPN11* in juvenile myelomonocytic leukemia, myelodysplastic syndromes and acute myeloid leukemia. *Nat. Genet.* **34**, 148–150 (2003).
44. Ostman, A., Hellberg, C. & Bohmer, F.D. Protein-tyrosine phosphatases and cancer. *Nat. Rev. Cancer* **6**, 307–320 (2006).
45. Dubé, N. *et al.* Genetic ablation of protein tyrosine phosphatase 1B accelerates lymphomagenesis of p53-null mice through the regulation of B-cell development. *Cancer Res.* **65**, 10088–10095 (2005).
46. Mullighan, C.G. Genome sequencing of lymphoid malignancies. *Blood* **122**, 3899–3907 (2013).
47. Kimura, Y., Morita, S.Y., Matsuo, M. & Ueda, K. Mechanism of multidrug recognition by MDR1/ABCB1. *Cancer Sci.* **98**, 1303–1310 (2007).
48. Zhang, H. *et al.* Downregulation of gene *MDR1* by shRNA to reverse multidrug-resistance of ovarian cancer A2780 cells. *J. Cancer Res. Ther.* **8**, 226–231 (2012).

ONLINE METHODS

Patient samples and cell lines. Specimens from 77 PMBCL and 30 Hodgkin lymphoma cases were selected from the tissue archives of the Centre for Lymphoid Cancer of the British Columbia Cancer Agency, the Arizona Lymphoma Repository and the Hôpital Henri Mondor Pathology Department according to the availability of fresh-frozen lymphoid tissue biopsy material and clinical patient follow-up data. Of these, two PMBCL specimens with an available source of matched constitutional DNA were used for whole-genome sequencing analysis. Seven PMBCL specimens, including the two cases from whole-genome sequencing, together with PMBCL-derived cell lines U-2940, MedB-1 and KARPAS-1106P, were used for RNA-seq. The clinical characteristics of the study cohort stratified by *PTPN1* mutational status are shown in **Supplementary Table 11a**,**b**. Ethical approval for this study was obtained from the University of British Columbia–British Columbia Cancer Agency Research Ethics Board (UBC BCCA REB) in accordance with the Declaration of Helsinki. HRS cells from Hodgkin lymphoma tissue biopsies were enriched by laser microdissection and underwent whole-genome amplification. All mutations found by whole-genome amplification were validated in DNA from microdissected HRS cells by nested PCR without amplification. Cell lines KM-H2, L-428, L-540, U-H01, SUP-HD1, HDLM-2, HD-MY-Z, L-1236, L-591, U-2940 and KARPAS-1106P were obtained from the German Collection of Microorganisms and Cell Cultures (DSMZ) and were propagated according to standard conditions. Cell line MedB-1 was a kind gift from S. Brüderlein and P. Möller (University of Ulm) and was propagated as published[49].

Whole-genome, deep amplicon and transcriptome sequencing. Whole-genome sequencing was performed as described[14]. In brief, genomic DNA was extracted using AllPrep DNA/RNA extraction kits (Qiagen). DNA was sheared by sonication, and the fraction of 350–450 bp in size was excised from a PAGE gel. Genome libraries were constructed using a modified paired-end protocol provided by Illumina, which included end repair, end preparation, adaptor ligation and ten cycles of PCR amplification of ligated fragments. The prepared library (10 nM) was sequenced on an Illumina HiSeq 2000 in 100-bp paired-end mode and aligned to the UCSC reference human genome (hg19) using Burrows-Wheeler Aligner[50]. JointSNVMix[51] was used to call SNVs and filter out calls with somatic probabilities of <0.8. Reported SNPs were removed using dbSNP (version 132). Additionally, MutationSeq[52] was applied to filter out SNVs with probabilities of <0.4, and annotations were added using SnpEff[53]. Only SNVs found in coding regions were reported in **Supplementary Table 1a**. Genomic rearrangements were predicted using deStruct, software derived from nFuse[54] that relies only on genomes, and were reported on the basis of whether (i) the rearrangement was a translocation, (ii) the breakpoint locations were within coding regions, (iii) the rearrangement probability was >0.5 and (iv) read support for the rearrangement was ≥5 in the tumor library and there was no read support in other libraries. Copy number estimation, alterations and somatic copy number aberrations in whole-genome high-throughput sequencing data were performed using HMMcopy[55].

For validation by deep amplicon sequencing of whole-genome sequencing predictions, amplicons were generated using a two-step PCR approach, with adaptor sequences added to gene-specific primers (**Supplementary Table 12**). PCR amplification was performed using 10 ng of genomic DNA and Q5 Hot-Start High-Fidelity DNA polymerase (NEB). Indexed PCR2 products were pooled and sequenced on an Illumina MiSeq instrument using the V2 300-cycles MiSeq reagent kit (Illumina), generating 150-bp paired-end reads.

Amplicon sequencing libraries were aligned to hg19 using Bowtie[56]. SAMtools mpileup was used to generate reference and variant reads at each position in each sample. A χ^2 test comparing the number of variant reads in the tumor compared to normal DNA was performed to test whether an SNV was somatic.

RNA-seq was performed as previously described[14]. In brief, double-stranded cDNA was synthesized from polyadenylated RNA and sheared. The fraction of 190–210 bp in size was isolated and amplified with ten cycles of PCR using the Illumina Genome Analyzer paired-end library protocol. Resulting RNA-seq libraries were sequenced on an Illumina Genome Analyzer II and aligned to hg19 using GSNAP[57]. Gene fusions were predicted using deFuse[58] and were reported on the basis of the following criteria: (i) altsplice = N, (ii) cDNA_breakseqs_percident < 0.5, (iii) breakseqs_estislands_percident < 0.5, (iv) genome_breakseqs_percident < 0.5, (v) break_adj_entropy_min > 0.5, (vi) probability > 0.5, (vii) one of the breakpoints was in a coding region and (viii) gene fusion partners were not adjacent. SNVs were called using SNVMix2 (ref. 59) and annotated using SnpEff[53]. Reported SNPs were removed using dbSNP (version 132). SNVs were reported on the basis of the following criteria for clinical samples: (i) the SNV affected a protein-coding gene, (ii) the SNV had a protein-coding effect, (iii) the probability of the non-reference allele was ≥0.8, (iv) ≥4 reads supported the variant allele and (v) ≤5% of the variant reads contained an indel. SNVs were reported on the basis of the following criteria for cell lines: (i) the SNV affected a protein-coding gene, (ii) the SNV had a protein-coding effect, (iii) the probability of the non-reference allele was ≥0.95, (iv) ≥6 reads supported the variant allele, (v) variant frequency was ≥45% and (vi) ≤1% of the variant reads contained an indel.

Laser microdissection of HRS cells. HRS cells were enriched by laser microdissection (Nikon eclipse TE2000-S microscope equipped with Molecular Machines Industries Technology) as follows. Sections (6 μm) from fresh-frozen tissue were mounted on membrane slides and fixed in 70% ethanol. Adjacent sections were also prepared on glass slides and were stained with hematoxylin and eosin to assess cell morphology and HRS cell content, which showed a wide range from only 1 cell per high-power field in HRS cell–poor cases to approximately 50 cells per high-power field in HRS cell–rich cases. Sections mounted on membrane slides for microdissection were stained with hematoxylin for 20 s, and 500–1,000 individually picked cells per case were excised and lysed in cell lysis solution (Puregene Core Kit A, Qiagen) for subsequent DNA extraction and whole-genome amplification. On average, 4 consecutive sections were needed per case to obtain the required number of HRS cells (range of 2–8 sections).

DNA extraction and whole-genome amplification. Genomic DNA from PMBCL clinical specimens and 500–1,000 pooled HRS cells per case were extracted using Allprep DNA/RNA extraction kits (Qiagen) and Puregene Cell & Tissue kits by Gentra Systems, respectively. Proteinase K digestion was carried out overnight, and glycogen (Invitrogen) was used as a DNA carrier. Whole-genome amplification was only performed on DNA extracted from HRS cells using the GenomePlex Whole-Genome Amplification kit (Sigma-Aldrich) to obtain >200 ng of amplified product per case. For quality control purposes, 50 ng of amplified DNA was analyzed by multiplex PCR (Qiagen) as previously described[60]. PCR was performed with five primer sets that produced fragments of 100, 200, 300, 400 and 600 bp from non-overlapping target sites in housekeeping genes[61]. Samples were classified on the basis of the largest of the five possible PCR products detected, and cases with at minimum the 300-bp product were used for further analysis. All mutations discovered by whole-genome amplification were confirmed by targeted nested PCR using DNA from freshly microdissected HRS cells to remove false positives.

Screening for *PTPN1* somatic mutations. *PTPN1* mutations in PMBCL were detected by Sanger sequencing (n = 49) and deep amplicon sequencing (n = 28). Mutations in Hodgkin lymphoma were detected by nested PCR followed by Sanger sequencing. For Sanger sequencing, primer sequences are listed in **Supplementary Table 13**. All ten *PTPN1* exons were amplified by standard PCR (Invitrogen) using primer set 1 (PMBCL) or primer sets 1 and 2 for nested PCR (HRS) and Sanger sequencing (3130 Genetic Analyzer, Applied Biosystems). Mutation analysis was performed using Clone manger software (Scientific & Educational Software). For deep amplicon sequencing, we used the Illumina TruSeq Custom Amplicon (TSCA) protocol according to the manufacturer's instructions, covering the complete protein-coding sequence of *PTPN1*. Amplicon libraries were sequenced on an Illumina MiSeq instrument using the V2 300-cycles MiSeq reagent kit (Illumina), generating 150-bp paired-end reads. Data analysis was performed as described above.

Analysis of tissue sections by immunohistochemistry. Immunohistochemistry was performed on formalin-fixed, paraffin-embedded tissue and fresh-frozen samples of Hodgkin lymphoma (n = 215) and PMBCL (n = 143) that included previously published cases represented on a tissue microarray (TMA)[16,62]. Whole-tissue sections of selected cases were stained and are shown in **Figure 3**. TMAs and sections were stained with an antibody to PTP1B (04-1140, Millipore) using routine protocols for automated procedures on

doi:10.1038/ng.2900

the Ventana Benchmark XT (Ventana Medical Systems). Scoring was performed by K.L.T., A.M. and R.D.G., and the percentage of tumor cells that were positive for PTP1B was recorded. For Hodgkin lymphoma, CD30 immunohistochemistry was used as a reference to identify HRS cells.

Quantitative RT-PCR. TaqMan gene expression assay probes were used to detect the mRNA levels of *PTPN1* (Hs00182260_m1), *BCL6* (Hs00277037_m1) and *MYC* (Hs00905030_m1) on a 7900HT RT-PCR system (Applied Biosystems). *GAPDH* was run as an internal control. Measurements were quantified using the $\Delta\Delta C_t$ method (Pfaffl) and expressed relative to the expression in non-silencing cells.

FISH analysis. FISH analysis was performed according to standard protocols with cells fixed with Carnoy's solution for cell lines, on PIN (paraffin-isolated nuclei) for PMBCL clinical samples and FICTION (Fluorescence Immunophenotyping and Interphase Cytogenetic as a Tool for Investigation Of Neoplasia) for Hodgkin lymphoma cases. For *PTPN1* copy number detection, a dual-color probe was designed using in-house BAC clones (CTD-2582P13) for 20q13.3 labeled in spectrum orange and telomere 20p13 (Abbott Molecular) as a control labeled in spectrum green. Slides were analyzed using a Zeiss Axioplan 2 fluorescence microscope (Zeiss Gollingen) and documented using an ISIS imaging system (Metasystems). One hundred interphase nuclei were scored for *PTPN1* copy number.

***PTPN1* silencing by lentiviral-mediated RNA interference.** Stable knockdown of *PTPN1* transcript in Hodgkin lymphoma cell line KM-H2 (KMH2-PTPN1-KD) was generated by lentiviral transduction with a vector expressing shRNA (pGIPZ-shPTPN1, clone V2LHS_262177, Open Biosystems) that, after processing to mature small interfering RNA (siRNA), interferes with *PTPN1* exon 10. Cells transduced with a vector with a non-interfering shRNA insert (pGIPZ non-silencing lentiviral shRNA control, RHS4346, Open Biosystems) were used for comparison (KMH2-NS).

For lentivirus production, shRNAmir constructs were cotransfected into HEK 293T cells with Trans-Lentiviral Packaging Mix (Open Biosystems; containing pTLA1-Pak, pTLA1-Enz, pTLA1-Env, pTLA1-Rev and pTLA1-TOFF) by lipid-mediated transfection (Arrest-In, Open Biosystems, Thermo Scientific). Supernatant was collected 48 and 72 h after transfection and concentrated by ultracentrifugation (Optima, Beckman) for 1.5 h at 65,000g at 4 °C. Lentiviral particles were resuspended in RPMI and used for the transduction of KM-H2 cells. Wild-type cells were transduced by adding 4 μg/ml polybrene (final concentration) with both pGIPZ-shPTPN1 virus and non-silencing control virus. GFP-positive cells were sorted on a BD FACSAria cell sorter (BD Biosciences) 3–5 d after transduction and were cultured using standard techniques. Efficiency of knockdown was evaluated by measuring the residual expression of the transcript by qRT-PCR.

Expression of PTP1B mutants and *SEAP* reporter gene assays. The *PTPN1* coding sequence was amplified by PCR using cDNA from KM-H2 (wild type), L-1236 (p.Gln9*), MedB-1 (p.Arg156*), PM-5 (p.Ala69Val), HD-MY-Z (p.Met74Leu), PM-7 (p.Val184Asp) and L-428 (p.Met282Leu) and cloned into the mammalian expression vector pcDNA3.1 (Invitrogen). Empty pcDNA3.1 (MT) was used as a mock vector. Plasmids were purified by Spin miniprep kit (Qiagen), and 2.5 μg of each plasmid was transfected into HEK 293 cells expressing STAT6 (HEK 293–STAT6; HEK blue IL4/IL13, Invivogen) using Lipofectamine 2000 (Invitrogen). Transfected cells were cultured for 48 h, and secreted embryonic alkaline phosphatase (SEAP) levels were assayed in culture supernatant according to the manufacturer's protocol. A plasmid encoding GFP was used to determine equal transfection efficiency (>90%).

Cell lysis and protein blotting. Total cell lysates were prepared from cultured cell lines treated with or without 10 ng/ml (for KMH2-PTPN1-KD cells) and 20 ng/ml (for HEK 293-STAT6 cells) recombinant human IL-4 (R&D Systems) for 10 min at 37 °C using mammalian protein extraction reagent (M-PER, Thermo Scientific) and in the presence of a protease inhibitor cocktail (Sigma-Aldrich). Protein lysates (25 μg) were resolved on a 4–12% NuPAGE Novex Bis-Tris gradient gel (Invitrogen) and transferred to a nitrocellulose membrane (Thermo Scientific) by semidry transfer (Bio-Rad) and probed with the following primary antibodies at 1:1,000 dilutions: PTP1B (AE4-2J, EMD); JAK1 (3332), phospho-JAK1 (3331), JAK2 (3230), phospho-JAK2 (3776), STAT3 (9132), phospho-STAT3 (9134), phospho-STAT5 (9359), phospho-STAT6 (9364), AKT (4511), phospho-AKT (4058) (all from Cell Signaling Technology); STAT5 (sc-835, Santa Cruz Biotechnology); and STAT6 (ab32108, Abcam). Antibody to β-actin (A5441, Sigma-Aldrich) was used as an internal control. Appropriate horseradish peroxidase (HRP)-conjugated secondary antibodies to rabbit or mouse IgG (W401B and W402B, respectively, Promega) were used at 1:10,000 dilutions to visualize bands with the enhanced chemiluminescence (ECL) system (Amersham) on an X-OMAT 2000A film processor (Kodak) or a Chemidoc digital imager (Bio-Rad). Intensities of developed bands were quantified using ImageJ software (US National Institutes of Health).

PTP1B activity assays. Phosphatase activity of prepared cell lysates from HEK 293–STAT6 cells expressing wild-type or mutant PTP1B were assayed using the Duoset IC Human Active PTP1B kit (R&D Systems) according to the manufacturer's instructions. Sodium orthovanadate (Na_3VO_4) was used as a tyrosine phosphatase inhibitor.

Gene expression profiling. RNA was extracted from duplicate KMH2-PTPN1-KD and KMH2-NS cultures and hybridized on Human Genome U133 Plus 2.0 microarrays (Affymetrix). Output was processed using the Robust Multi-array Average method. Probe-set fold-change differences represent average expression in knockdown versus non-silencing samples. The binomial sign test was performed using the "binom test" function (R Project). Genes with a fold change of >1.25 or <0.8 were considered to be differentially expressed and are reported. Molecular pathway and gene set enrichment analyses of differentially expressed genes were performed using Ingenuity Pathway Analysis (Ingenuity Systems), GSEA (2.0.13) and the Molecular Signatures Database (4.0, Broad Institute).

Statistical analysis. Comparisons between groups were performed using two-sample Student *t* tests. Time-to-event analyses were performed using the Kaplan-Meier method, and survival curves were compared by the log-rank test using SPSS Version 14.0. Disease-specific survival (DSS) was defined as the time elapsing from diagnosis to last follow-up or death due to lymphoma. Overall survival (OS) was defined as the time from diagnosis to death from any cause. Progression-free survival (PFS) was defined as the time from diagnosis to progression (relapse after primary treatment, initiation of new treatment or death from any cause). Treatment failure was defined as the time from primary treatment to progression.

49. Möller, P. *et al.* MedB-1, a human tumor cell line derived from a primary mediastinal large B-cell lymphoma. *Int. J. Cancer* **92**, 348–353 (2001).
50. Li, H. & Durbin, R. Fast and accurate long-read alignment with Burrows-Wheeler transform. *Bioinformatics* **26**, 589–595 (2010).
51. Roth, A. *et al.* JointSNVMix: a probabilistic model for accurate detection of somatic mutations in normal/tumour paired next-generation sequencing data. *Bioinformatics* **28**, 907–913 (2012).
52. Ding, J. *et al.* Feature-based classifiers for somatic mutation detection in tumour-normal paired sequencing data. *Bioinformatics* **28**, 167–175 (2012).
53. Cingolani, P. *et al.* A program for annotating and predicting the effects of single nucleotide polymorphisms, SnpEff: SNPs in the genome of *Drosophila melanogaster* strain *w1118*; *iso-2*; *iso-3*. *Fly (Austin)* **6**, 80–92 (2012).
54. McPherson, A. *et al.* nFuse: discovery of complex genomic rearrangements in cancer using high-throughput sequencing. *Genome Res.* **22**, 2250–2261 (2012).
55. Ha, G. *et al.* Integrative analysis of genome-wide loss of heterozygosity and monoallelic expression at nucleotide resolution reveals disrupted pathways in triple-negative breast cancer. *Genome Res.* **22**, 1995–2007 (2012).
56. Langmead, B., Schatz, M.C., Lin, J., Pop, M. & Salzberg, S.L. Searching for SNPs with cloud computing. *Genome Biol.* **10**, R134 (2009).
57. Wu, T.D. & Nacu, S. Fast and SNP-tolerant detection of complex variants and splicing in short reads. *Bioinformatics* **26**, 873–881 (2010).
58. McPherson, A. *et al.* deFuse: an algorithm for gene fusion discovery in tumor RNA-Seq data. *PLOS Comput. Biol.* **7**, e1001138 (2011).
59. Goya, R. *et al.* SNVMix: predicting single nucleotide variants from next-generation sequencing of tumors. *Bioinformatics* **26**, 730–736 (2010).
60. van Beers, E.H. *et al.* A multiplex PCR predictor for aCGH success of FFPE samples. *Br. J. Cancer* **94**, 333–337 (2006).
61. van Dongen, J.J. *et al.* Design and standardization of PCR primers and protocols for detection of clonal immunoglobulin and T-cell receptor gene recombinations in suspect lymphoproliferations: report of the BIOMED-2 Concerted Action BMH4-CT98-3936. *Leukemia* **17**, 2257–2317 (2003).
62. Steidl, C. *et al.* Tumor-associated macrophages and survival in classic Hodgkin's lymphoma. *N. Engl. J. Med.* **362**, 875–885 (2010).